"Synthesis of Schiff base crosslinked polyaniline hydrogels with enhanced electrochemical performance for supercapacitor applications".

Samaresh Ghosh, Jagannath Majhi, Sonal Sharma, Kumari Priya, Anasuya Bandyopadhyay*

Department of Polymer & Process Engineering, IIT Roorkee, Saharanpur Campus, Saharanpur-247001, India
Email: anasuya.bandyopadhyay@pe.iitr.ac.in

1. Characterizations

Structural analysis of the prepared crosslinker was done by FTIR and NMR spectroscopy. The FTIR spectra of the synthesized crosslinker molecule and PANI aerogel were recorded using KBr pellets in a PerkinElmer spectrophotometer instrument (L1600400 Spectrum TWO DTGS, UK). ^{1}H-NMR data of all the small synthesized molecules were collected from Bruker (AVANCE III) operated at 500 MHz with deuterated dimethyl sulfoxide (DMSO-D6) solvent. All the NMR study was carried out at room temperature using tetramethyl silane (TMS) as an internal reference. FESEM was done to analyze the morphology of the synthesized gel and the effect of crosslinker on morphology. FESEM image was taken from TESCAN MIRA3 after gold coating, and the instrument was operated at 5 to 40 kV. AFM images taken from NT-MDT-INTEGRA microscope. UV-absorbance spectra were analyzed after dispersing the hydrogel in DMSO as solvent. The data was taken from the Agilent, CARY 5000, at room temperature. Wide-angle X-ray diffraction data of the dried hydrogel was taken from the RIGAKU ULTIMA IV X-ray diffractometer machine operating at 40 kV. The scanning was done from 5 to 80 degrees at a scan rate of 4° per minute. RAMAN spectra were recorded using a Raman microscope via confocal mode (Renishaw, UK) under a 785 nm monochromatic laser. The surface area of the synthesized aerogel was measured by an N_2 adsorption/desorption isotherm experiment using a Quantachrome Autosorb analyzer. BET study was done after degassing the sample for 13 hrs. at a high temperature of 415K. Pore size and distribution were measured through the NLDFT (Nonlinear Density

Functional Theory) method. To understand the rheological properties of the hydrogel, rheological tests have been carried out with an advanced rheometer (Anton Par) (MCR102SN111111). The hydrogel sample was placed in between two parallel plates, and the frequency was varied from 0.1 to 100 Rad/s. The thermal stability of the synthesized PANI aerogel was investigated using thermogravimetric analysis (TGA) on TA Instruments (TGA55, Discovery series) in an open atmosphere. The temperature range was set from 30 °C to 800 °C at a scan rate of 10°C/min.

Specific capacitance (C) in a three-electrode system is calculated from both CV and GCD by utilizing the following equations-

$$C = \int idV / (2 * m * sr * \Delta V) \quad \text{..... 1}$$

Where C = specific capacitance (F/g), $\int idV$ = area under curve of CV, sr – scan rate, ΔV = Potential window.

$$C = I\,\Delta t\,/m\,\Delta V \quad \text{..... 2}$$

Where I = Current (A), Δt = discharge time (s), m = mass loaded on GC electrode (mg), ΔV = potential window (V)

The areal capacitance (C_s, mF/cm^2), energy density (E, µWh/cm^2), and power density (P, µW/cm^2) of the symmetric supercapacitor are calculated by the above formula.[1,2]

Areal capacitance $Cs = I\Delta t/S\Delta V$

Energy density $E = \left(C.\frac{\Delta V^2}{2}\right) * 10/36$ 3

Power density $P = E * 3600/\Delta t$ 4

Where I = Current (A), Δt = discharge time (s), S = coated area (cm^2), ΔV = potential window (V).

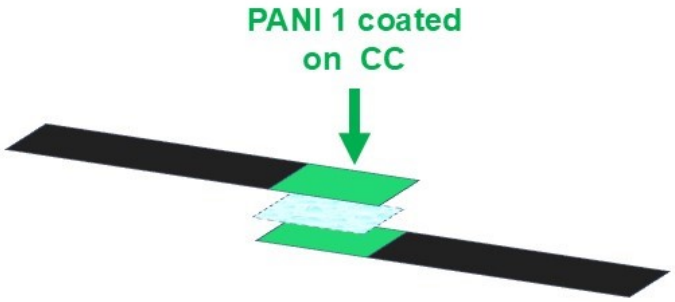

Scheme S1 Schematic representation of fabricated symmetric supercapacitor

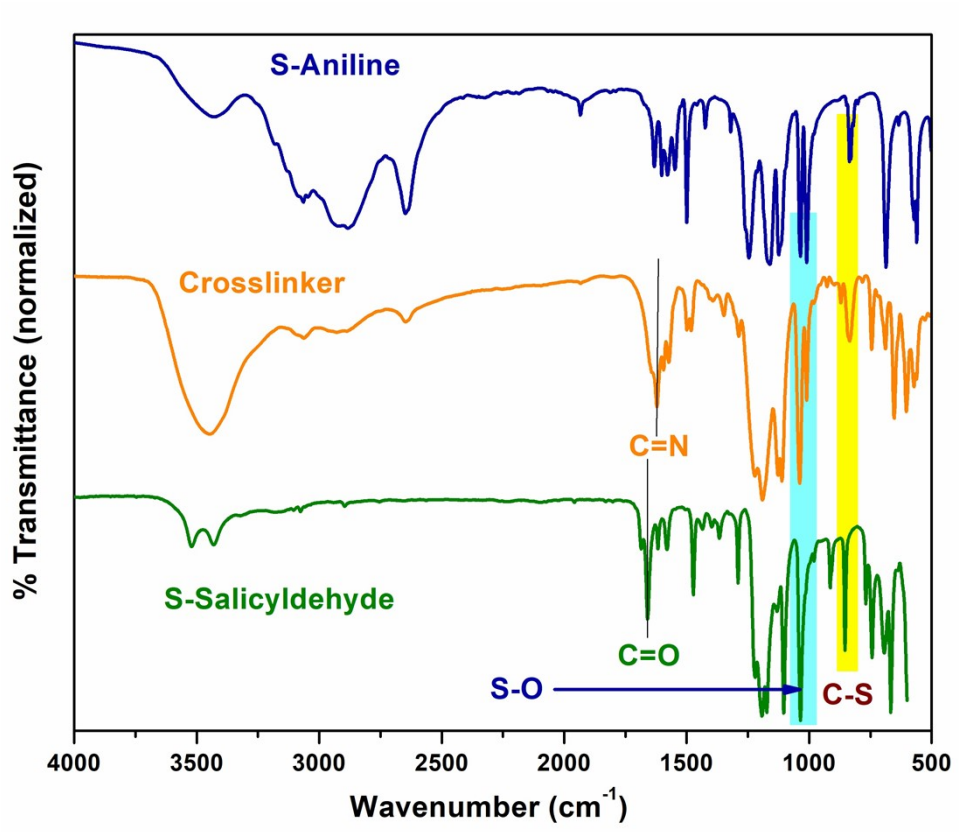

Fig. S1 Overlaid FTIR spectra of the synthesized crosslinker with two precursors.

Wavenumber (cm^{-1})	Corresponding Bond
1660	$\nu_{C=O}$
1621	$\nu_{C=N}$
1038	ν_{S-O}
835	ν_{C-S}

Table S1 Characteristic peaks of crossliker.

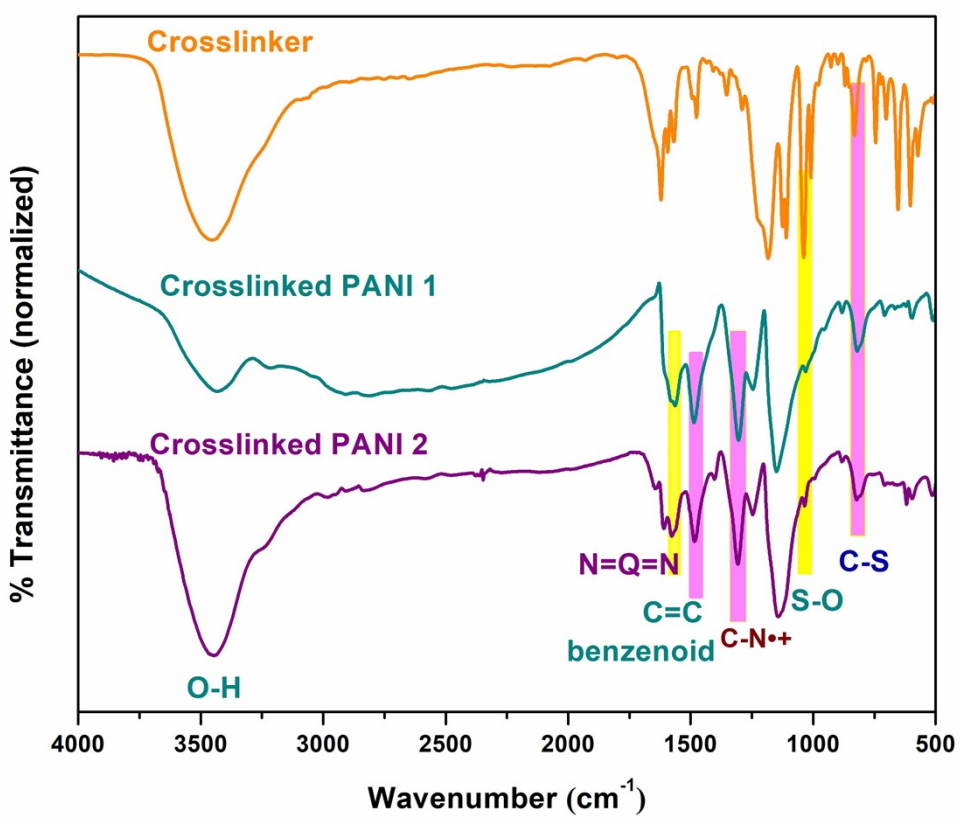

Fig. S2 Overlaid FTIR spectra of synthesized crosslinked PANI 1, PANI 2, and crosslinker

Wavenumber (cm^{-1})	Corresponding Bond
1569	$\nu_{C=C}$ of benzenoid
1486	$\nu_{C=N}$ of quinone ring
1303	ν_{C-N+}
1030	ν_{S-O}
817	ν_{C-S}

Table S2 Significant peaks of the PANI 1 and PANI 2.

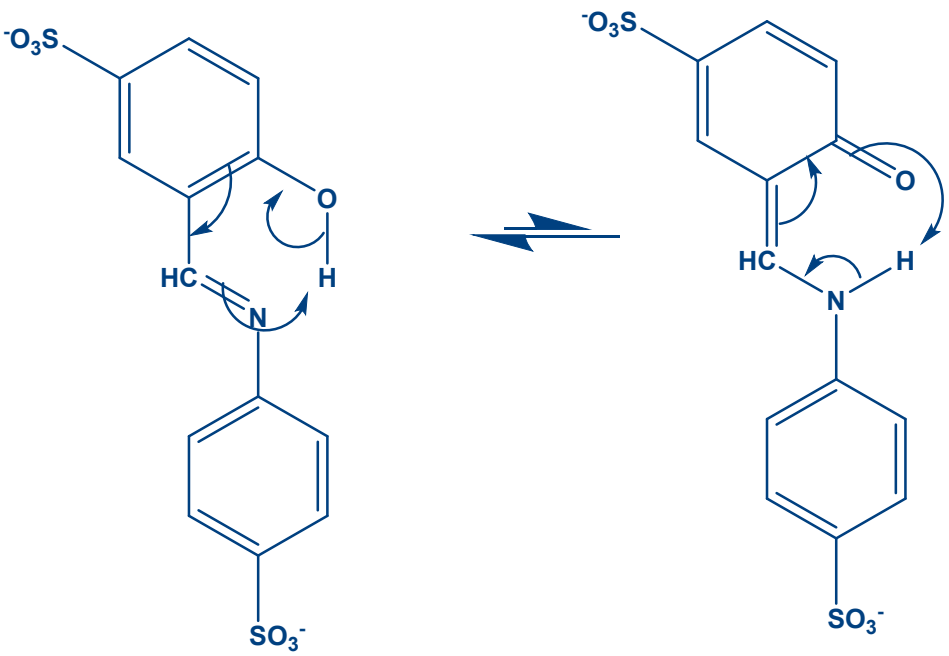

Scheme S2 Tautomerism between imine-ol to keto-enamine forms

a)

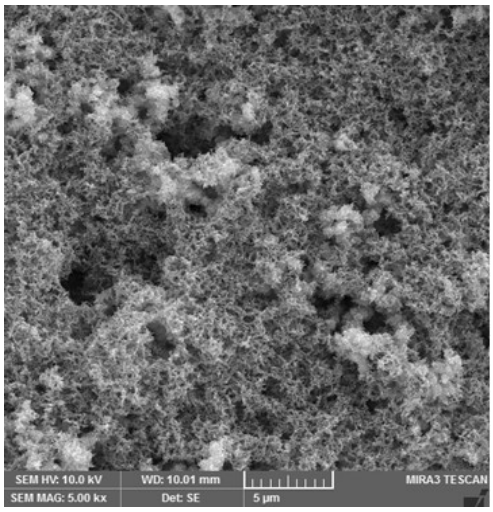
SEM HV: 10.0 kV
WD: 10.01 mm
MIRA3 TESCAN
SEM MAG: 5.00 kx
Det: SE
5 µm

b)

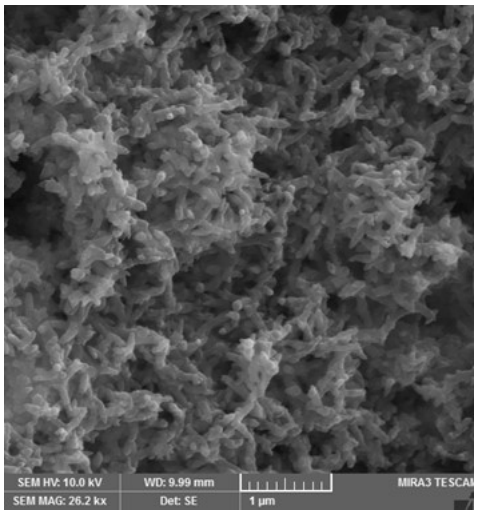
SEM HV: 10.0 kV
WD: 9.99 mm
MIRA3 TESCAN
SEM MAG: 26.2 kx
Det: SE
1 µm

c)

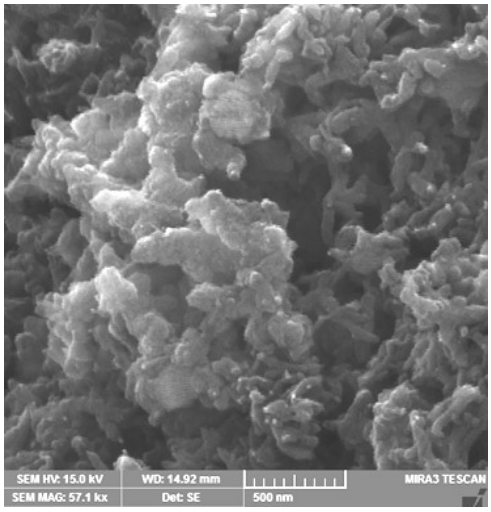
SEM HV: 15.0 kV
WD: 14.92 mm
MIRA3 TESCAN
SEM MAG: 57.1 kx
Det: SE
500 nm

d)

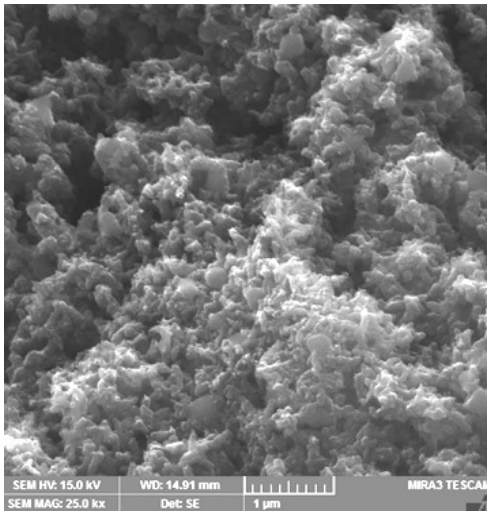
SEM HV: 15.0 kV
WD: 14.91 mm
MIRA3 TESCAN
SEM MAG: 25.0 kx
Det: SE
1 µm

e)

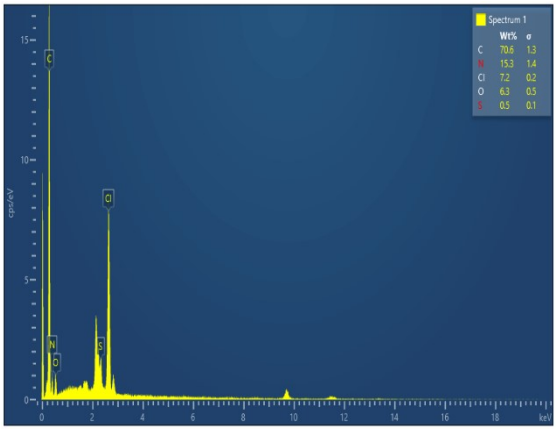
Spectrum 1
Wt%
C 70.6
N 15.3
Cl 7.2
O 6.3
S 0.5
cps/eV
keV

Fig. S3 (a) and (b)FESEM images of PANI 1 at different resolutions. (c) and (d) FESEM images of PANI P at different resolutions. (e) EDAX of PANI 1.

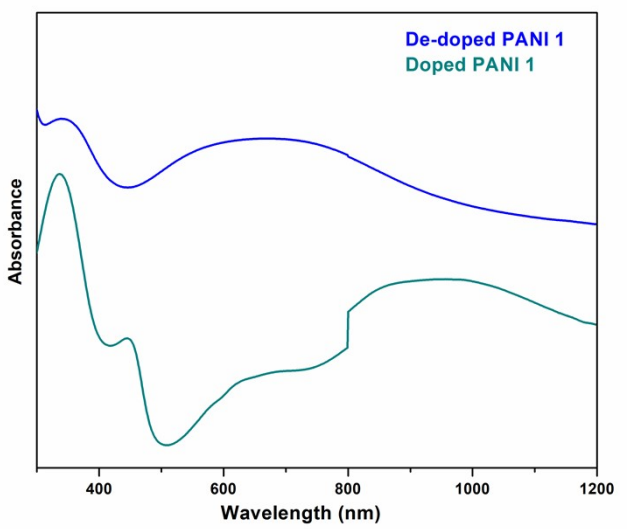

Fig. S4 Overlaid UV-Vis-NIR spectra of doped and de-doped Crosslinked PANI 1.

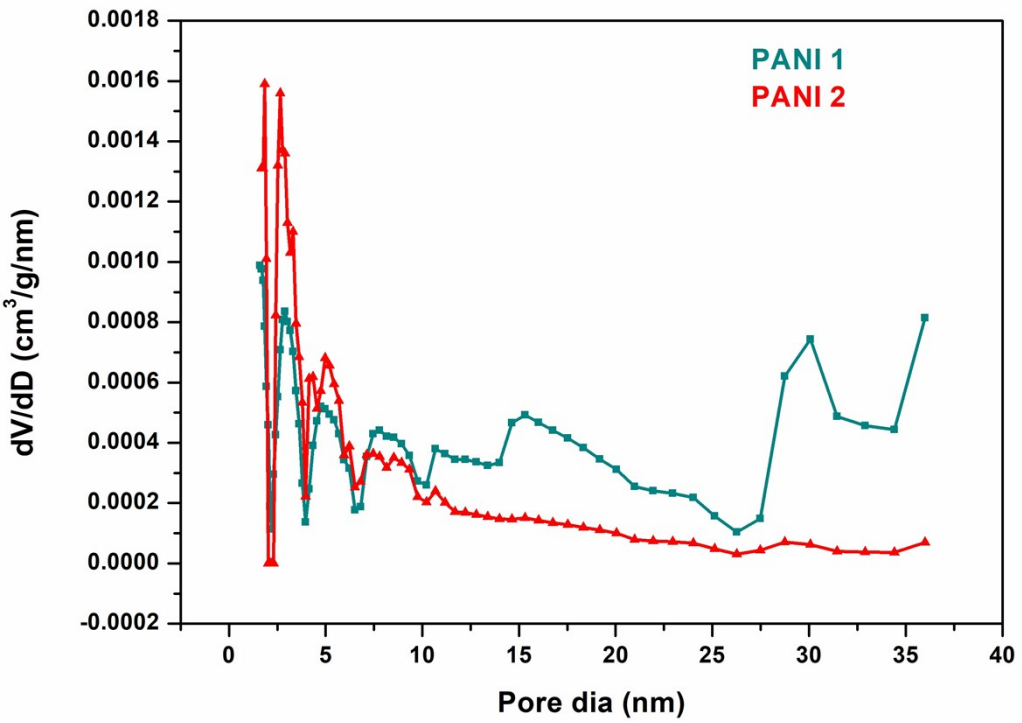

Fig. S5 Pore size distribution of PANI 1 and PANI 2

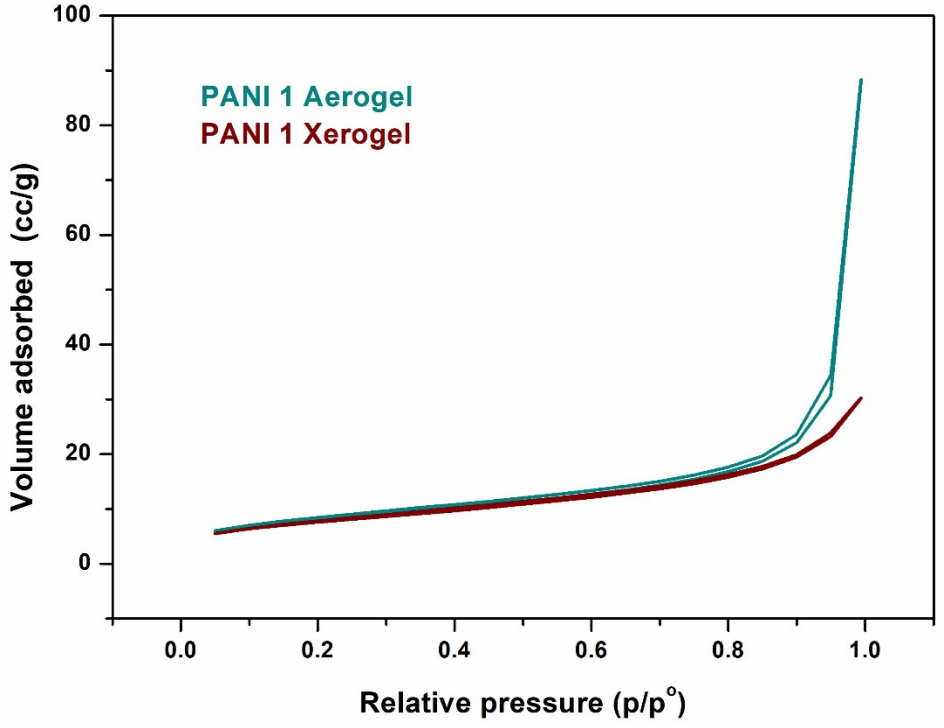

Fig. S6 N_2 Adsorption-desorption of PANI 1 aerogel and xerogel.

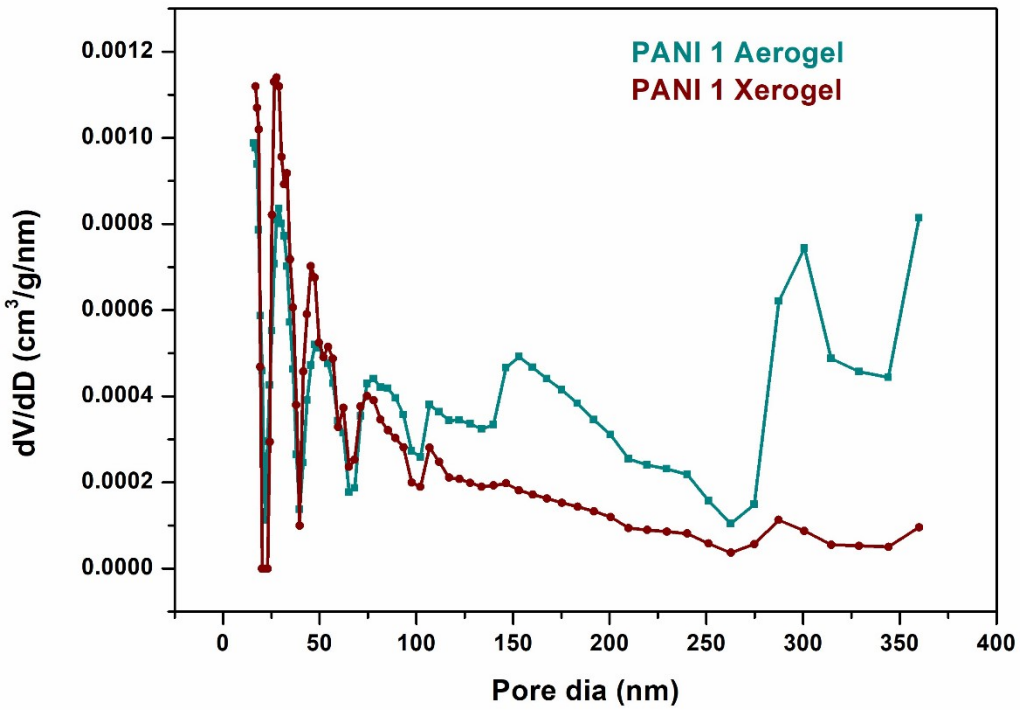

Fig. S7 Pore size distribution of PANI 1 aerogel and xerogel

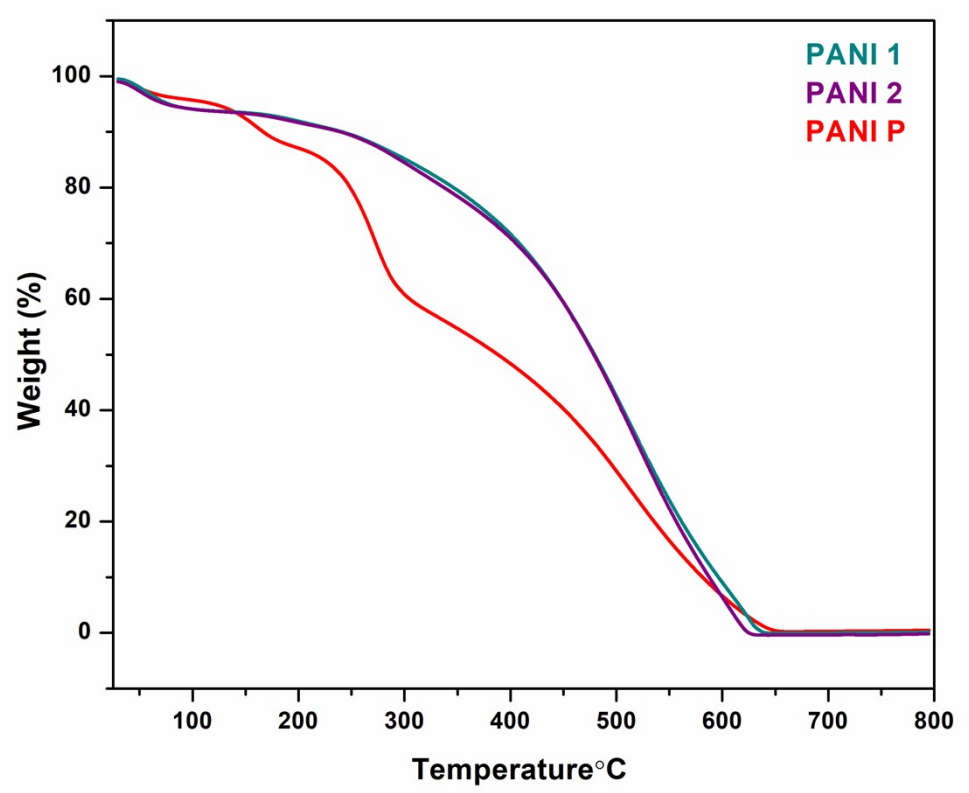

Fig. S8 TGA analysis of PANI 1, PANI 2, and PANI P.

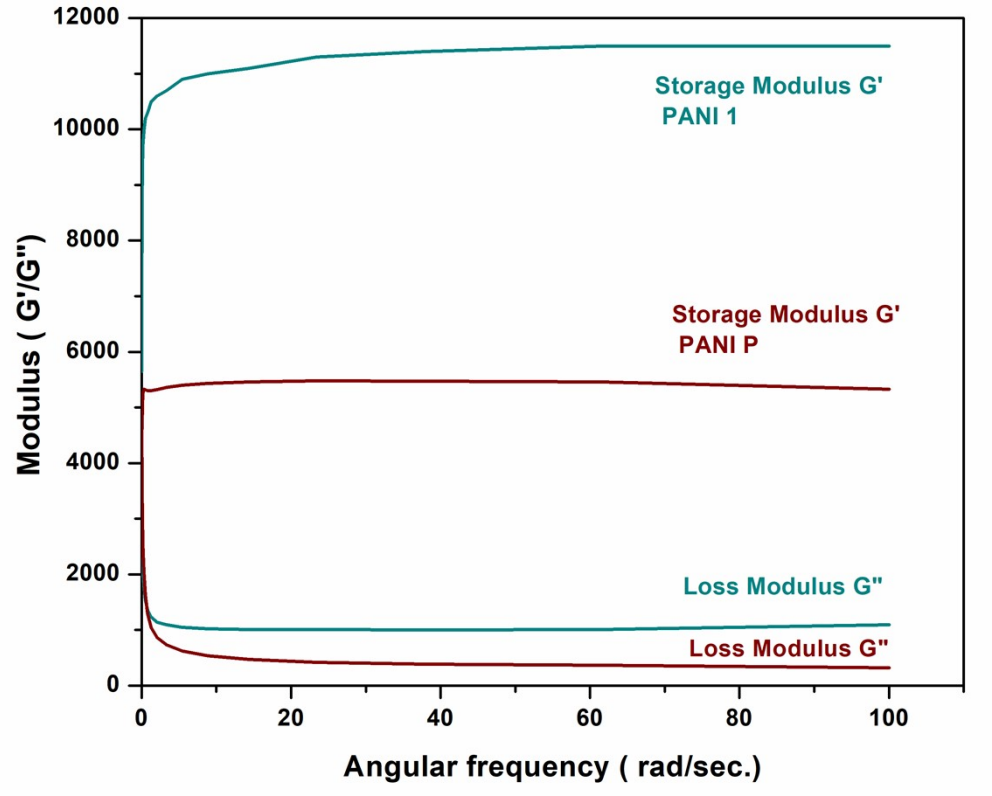

Fig. S9 The frequency dependence of the storage modulus G′ and the loss modulus G″ of crosslinked PANI and crosslinker-free PANI.

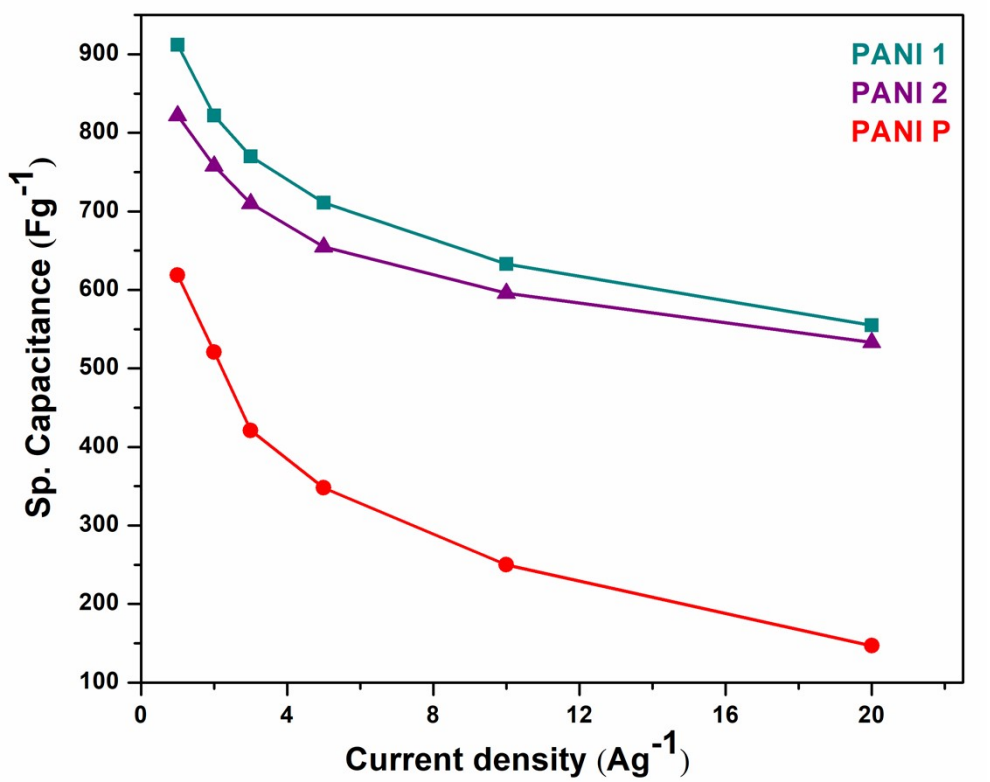

Fig. S10 Comparison of rate capability of PANI 1, PANI 2, and PANI P in 1M H_2SO_4 electrolyte.

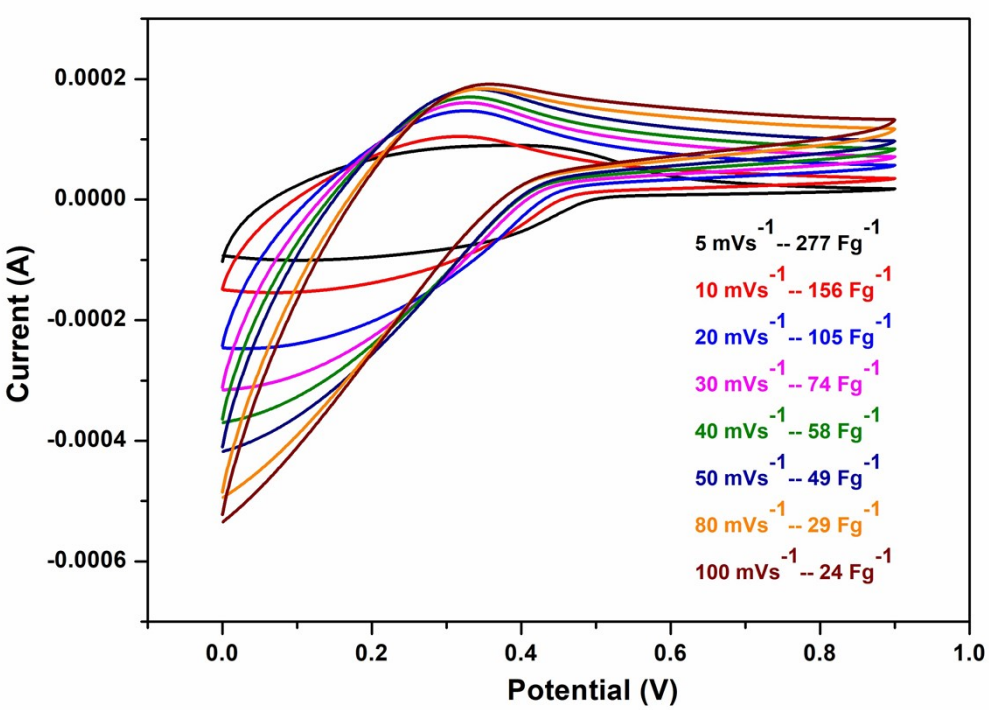

Fig. S11 CV of crosslinked PANI 1 aerogel in 1M Na_2SO_4 electrolyte

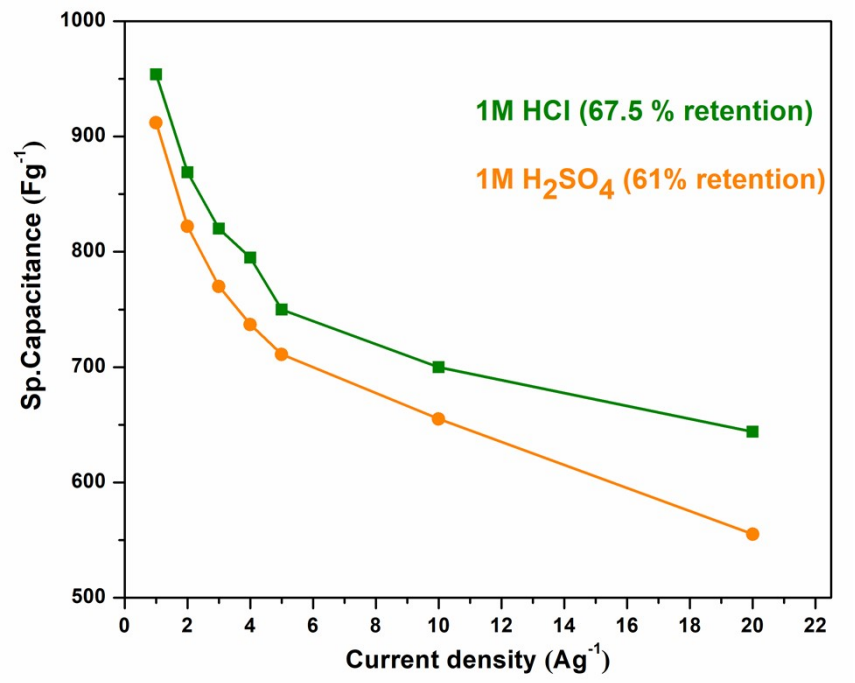

Fig. S12 Comparison of rate capability of PANI 1 aerogel in two different electrolytes.

Sample	$R_1=R_S$	$R_2=R_{CT}$	CPE 1-T	CPE 1-P	Equivalent circuit
Crosslinked PANI 1	3.431	61.12	0.00018676	0.67682	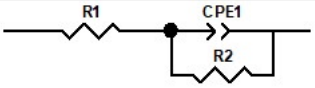
Crosslinked PANI 1	3.505	219.4	0.00012639	0.70958	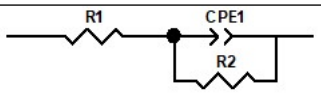
PANI P	4.536	243	$5.1075E^{-05}$	0.80036	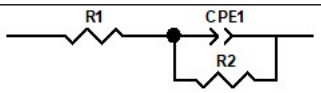

Table S3 Fitted parameters after simulation of EIS data through Zview

From CV			From GCD	
Scan rate (mVs^{-1})	Areal capacitance (mF/cm^2)	Gravimetric Capacitance (Fg^{-1})	Current Density (mA/cm^2)	Areal Capacitance (mF/cm^2)
10	796	114	1	480
20	612	88	2	455
30	494	70	3	437
50	337	48	5	411
100	173	25	10	355

Table S4: Areal and Gravimetric capacitance calculation from CV and GCD of the symmetric supercapacitor

Active Material	Electrolyte	Areal Capacitance (mF/cm^2)	Energy density (ED)	Cycling stability	Ref.
PANI/PAM	PAM/phytic acid	343 mF/cm^2 at 1.25 mA/cm^2	17.2 $\mu Wh/cm^2$	80 % retained after 2000 cycles	[3]
PANI/Mxene	PVA/H_2SO_4	710 mF/cm^2 at mA/cm^2	0.063 mWh/cm^2	61.5 % retained after 10000 cycles at 5 mA/cm^2	[4]
PANI@$Ti_3C_2T_x$/PVA	PVA/H_2SO_4	103.8 mF/cm^2 at 0.2 mA/cm^2	9.2 $\mu Wh/cm^2$	99.5 % retained after 10000 cycles at 75 A/m^2	[5]
PANI/Mxene/CNF	PVA/H_2SO_4	522 mF/cm^2 at 5 mA/cm^2	94.7 $\mu Wh/cm^2$	81.5 % retained after 4000 cycles	[6]
PANI/PVA	1M H_2SO_4	86 Fg^{-1} at $1Ag^{-1}$		95 % retained after 1000 cycles at $5Ag^{-1}$	[7]
PANI/HQ/PVA	PVA/H_2SO_4		12 Wh/kg.	77.6% up to 10 000 @ 1.5 A/g	[8]
PANI/Graphene	PVA/H_2SO_4	453 mF/cm^2 at $5mVs^{-1}$	9.4 mWh/cm^3	90% after 3000 @ 100 mvs	[9]
PANI/PVA/PAAM	PVA/PAAM/H_2SO_4	250.75 mF/cm^2	34.8 $\mu Wh/cm^2$	90.03% retained after 5000 cycles	[10]
PANI/PVA-PAM/AA	PVA/H_2SO_4-glycerol	95.8 mF/cm^2. @0.2 mA/cm^2	8.5 $\mu Wh/cm^2$	89.6% capacitance retained after 40000 cycles	[11]
PANI/cellulose/Fe^{3+}	PVA/H_2SO_4	185 mF/cm^2 at 0.2 mA/cm^2	6.5 $\mu Wh/cm^2$	79 % capacitance retained after1000 cycles at 0.6 mA/cm^2	[12]
100% PANI	**PVA/H_2SO_4**	**480 mF/cm^2 at 1mA/cm^2**	**54 $\mu Wh/cm^2$**	**74 % capacitance retained after1000 cycles at 5 mA/cm^2**	**This Work**

Table S5 Comparison table between previously published data and the electrochemical performance of a supercapacitor based on our developed crosslinked PANI 1 aerogel.

References:

1 L. Qin, G. Yang, D. Li, K. Ou, H. Zheng, Q. Fu and Y. Sun, *Chem. Eng. J.*, 2022, **430**, 133045.

2 N. Kamboj, T. Purkait, M. Das, S. Sarkar, K. S. Hazra and R. S. Dey, *Energy Environ. Sci.*, 2019, **12**, 2507–2517.

3 J. Zhao, G. Ji, Y. Li, R. Hu and J. Zheng, *Chem. Eng. J.*, 2021, **420**, 129790.

4 Z. Chen, Y. Wang, J. Han, T. Wang, Y. Leng, Y. Wang, T. Li and Y. Han, *ACS Appl. Energy Mater.*, 2020, **3**, 9326–9336.

5 S. Cao, T. Zhao, Y. Li, L. Yang, A. Ahmad, T. Jiang, Y. Shu, Z. Jing, H. Luo, X. Lu and H. Zhang, *Ceram. Int.*, 2022, **48**, 15721–15728.

6 T. Yuan, Z. Zhang, Q. Liu, X. T. Liu, Y. N. Miao and C. li Yao, *Carbohydr. Polym.*, 2023, **304**, 120519.

7 L. S. Devi, R. P. Palathinkal and A. K. Dasmahapatra, *Polymer (Guildf).*, 2024, **293**, 126673.

8 L. Dou, S. Zhou, J. Ma, C. Zhao, P. Cui, S. Ye, P. Feng, X. Gu, S. Huang and X. Tao, *J. Mater. Chem. C*, 2023, **12**, 521–532.

9 Y. Qu, C. Lu, Y. Su, D. Cui, Y. He, C. Zhang, M. Cai, F. Zhang, X. Feng and X. Zhuang, *Carbon N. Y.*, 2018, **127**, 77–84.

10 R. Wang, D. Lei, H. Zhang, J. Liang, Z. Shang, L. Wan, Z. Li and C. Si, *Compos. Part B Eng.*, 2024, **275**, 111345.

11 J. Huang, S. Han, J. Zhu, Q. Wu, H. Chen, A. Chen, J. Zhang, B. Huang, X. Yang and L. Guan, *Adv. Funct. Mater.*, 2022, **32**, 1–14.

12 Z. Liu, J. Chen, Y. Zhan, B. Liu, C. Xiong, Q. Yang and G. H. Hu, *ACS Sustain. Chem. Eng.*, 2019, **7**, 17653–17660.